Theory of Pattern Formation of Metallic Microparticles in Poorly Conducting Liquids

I. S. Aranson[1] and M. V. Sapozhnikov[1,2]

[1]*Materials Science Division, Argonne National Laboratory, 9700 South Cass Avenue, Argonne, Illinois 60439, USA*
[2]*Institute for Physics of Microstructures, Russian Academy of Sciences, GSP-105, Nizhny Novgorod, 603000, Russia*
(Received 18 June 2003; revised manuscript received 23 December 2003; published 9 June 2004)

We develop a continuum theory of self-assembly and pattern formation in metallic microparticles immersed in a poorly conducting liquid in a dc electric field. The theory is formulated in terms of conservation laws for the densities of immobile particles (precipitate) and bouncing particles (gas) coupled to the Navier-Stokes equation for the liquid. This theory successfully reproduced the correct topology of the phase diagram and primary patterns observed in the experiment [Sapozhnikov *et al.*, Phys. Rev. Lett. **90**, 114301 (2003)]: static crystals, honeycombs, dynamic pulsating rings, and rotating multipetal vortices.

Electromagnetic manipulation and assembly of small particles in electrolytes constitutes one of the great hopes for nanotechnology [1] and the new generation of microfluidic devices [2]. Many industrial technologies face the challenge of handling such single- or multicomponent micro- and nanosize ensembles. The dynamics of conducting microparticles in the electric field in the air was studied in [3,4]. The phase transitions and clustering instability of the electrostatically driven conducting microparticles were found. In our recent work we reported the new dynamic phenomena occurring with microparticles in poorly conducting liquid subject to a strong electric field (up to 20 kV/cm) [5]. It was shown that small metallic particles immersed in a toluene-ethanol mixture in a dc electric field form a rich variety of novel phases: static honeycombs, two-dimensional crystals, dynamic multipetal vortices, and pulsating rings. The phenomena were attributed to the interaction between particles and the electrohydrodynamic (EHD) flows.

In this Letter we develop the theory of pattern formation and self-assembly of metallic microparticles in a poorly conducting liquid placed between two horizontal planar electrodes. The theory is formulated in terms of two depth-averaged conservation laws for the densities of immobile particles (precipitate) and bouncing particles (gas) coupled to the Navier-Stokes equation for a vertical component of the velocity of the liquid v_z, whereas horizontal velocity $v_\perp$ is obtained from the continuity condition. This theory successfully reproduces the topology of the phase diagram and primary patterns observed in the experiment: static crystal's honeycombs, and dynamic pulsating rings and vortices [5]. In the framework of our theory we demonstrate that the rotation of clusters is the result of a symmetry-breaking instability leading to the formation of the traveling wave at the cluster perimeter.

Model.—Schematics of the experimental setting is shown in the inset of Fig. 1. Our studies show that two major control parameters are the potential difference ΔU which determines the average electric field $E = -\Delta U/d$, d is the spacing between electrodes, and the concentration

c of the additive (e.g., ethanol) which characterizes the conductivity of the liquid. Following the analysis of Ref. [4], we describe the evolution of the particulate by the number density of the precipitate $\rho_p(\mathbf{r}, t)$ and bouncing particles (or gas) $\rho_g(\mathbf{r}, t)$, where $\mathbf{r} = (x, y)$ are horizontal coordinates. All the quantities are averaged over the vertical coordinate z. Since the total number of particles $N = \int(\rho_p + \rho_g)dxdy$ is conserved, the evolution of the particulate is described by the conservation laws

$$\partial_t \rho_p = \nabla \mathbf{J}_p + f, \qquad \partial_t \rho_g = \nabla \mathbf{J}_g - f. \qquad (1)$$

Here $J_{p,g}$ are the mass fluxes of precipitate and gas, respectively, and the function f describes gas/precipitate conversion which depends on $\rho_{p,g}$, electric field E, and local concentration c. The fluxes can be written as

$$\mathbf{J}_{p,g} = D_{p,g}\nabla\rho_{p,g} + \alpha_{p,g}(E)\mathbf{v}_\perp\rho_{p,g}[1 - \beta(E)\rho_{p,g}], \quad (2)$$
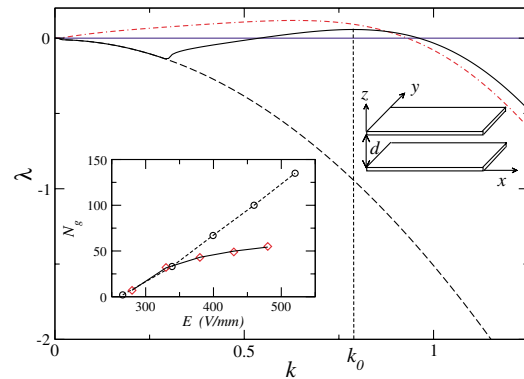

FIG. 1 (color online). The real part of λ vs k for three regimes: honeycomb (solid line, $E = -45$, $\beta = 2$, and $\kappa = -0.1$), coalescence (dot-dashed line $E = -55$, $\beta = 0.5$, and $\kappa = 0.1$), stable 2D crystal (dashed line, $E = 50$, $\beta = 2$, and $\kappa = -0.1$). Other parameters: $\zeta = 0.02$, $\bar{\rho} = 0.3$, $D_p = 1$, $\alpha_p = -\alpha_g = -0.3$, $\nu = 2$, $d_0 = 1$, and $\mu_0 = 0$. Insets: Experimental setup (right) and number of "gas" particles N_g vs E (left) with $N = 240$ (circles), $N = 70$ (diamonds); the solid line is fit $N_g \sim (E - E_0)N_s/N$.

where $D_{p,g}$ are precipitate/gas diffusivities. The last term, describing particles advection by fluid, is reminiscent of the Richardson-Zaki relation for drag force frequently used in the engineering literature [6]. The factor $[1 - \beta(E)\rho_{p,g}]$ describes the saturation of flux at large particle densities $\rho \sim 1/\beta$. Experiments show that at the onset of motion the maximum density in the patterns such as honeycombs is below submonolayer coverage whereas for large values of E the particles form multilayered structures. Thus β should decrease with the increase of E. According to the Richardson-Zaki relation, the coefficients $\alpha_{g,p}$ decrease with the increase of $\rho_{g,p}$ (i.e., void fraction). In order to mimic this effect on a qualitative level we assumed that $\alpha_{g,p}$ decreases with the increase of E (due to the increase of maximum density $\rho \sim 1/\beta$ with E). Since the gas is mostly concentrated near the upper electrode and the precipitate near the bottom, gas and precipitate are advected in *opposite directions*, i.e., the transport coefficients $\alpha_{p,g}$ have opposite signs. Since gas is more mobile than the precipitate, we set $D_g \gg D_p$. In the limit $D_g \rightarrow \infty$ and for $\alpha_{p,g} = 0$ one recovers the description of Ref. [4].

We assume that the vertical vorticity of the liquid $\Omega_z = \partial_x v_y - \partial_y v_x$ is small in comparison with the in-plane vorticity. This assumption is justified by the experimental observation that toroidal vortices create no or very small horizontal rotation. From $\Omega_z = 0$ one obtains

$$\mathbf{v}_\perp = -\nabla\phi, \qquad (3)$$

where ϕ is a "quasipotential." Substituting Eq. (3) into the continuity equation $\nabla\mathbf{v} = 0$ one expresses the quasipotential through the vertical velocity

$$\nabla^2\phi = \partial_z v_z. \qquad (4)$$

The vertical velocity v_z is obtained from the corresponding Navier-Stokes equation

$$\rho_0(\partial_t v_z + \mathbf{v}\nabla v_z) = \nu\nabla^2 v_z - \partial_z p + E_z q, \qquad (5)$$

where ρ_0 is the density of the liquid (we set $\rho_0 = 1$), ν is the viscosity, p is the pressure, and q is the charge density. The last term describes the electric force acting on the charged liquid. In order to average Eqs. (4) and (5) over the thickness of the cell $0 < z < d$, we assume that v_z is symmetric with respect to $d/2$ and $v_\perp$ is antisymmetric. Then after the averaging and taking into account that $\partial_z v_z = 0$ at $z = 0, d$ one obtains

$$\partial_t V = \nu\nabla^2 V - \zeta V - \Delta p + \langle E_z q\rangle, \qquad (6)$$

where $V = d^{-1}\int_0^d v_z dz$, and $\Delta p = p(d) - p(0)$. The term $-\zeta V$ accounts for a small dissipation due to friction between liquid, particles, and the walls of the container. Using the symmetry condition and integrating Eq. (4) over the lower half of the cell $(0 < z < d/2)$ one obtains

$$\nabla^2\Phi = a_0 V, \qquad (7)$$

where the constant $a_0 \sim O(1)$ can be scaled away and Φ is

averaged ϕ. The volume charge density $q \sim -c$ is negative and proportional to the additive concentration c, the vertical component of the electric field E_z depends on E and the local density of particles, $\rho_p + \rho_g$. Since the increase in the amount of conducting particles decreases the effective spacing between the electrodes and, therefore, increases the apparent electric field, one obtains

$$E_z \approx \frac{E}{1 - (\rho_p + \rho_g)/s} \sim E + E(\rho_p + \rho_g)/s, \qquad (8)$$

where the constant $s \approx d/r_0$, and r_0 is the particle diameter. After applying the divergence operator to the Navier-Stokes equation one finds that the pressure itself is a functional of $\langle Eq\rangle$ (compare with the Rayleigh-Benard convection, see, e.g., [7]). Because of the translation and rotation invariance of Eq. (6) in the most general form Δp can be written as $\Delta p = \int K(|\mathbf{r} - \mathbf{r}'|)\langle E_z q\rangle d\mathbf{r}'$. The kernel $K(r)$ has the property $\int K d\mathbf{r}' = 1$ since the uniform force distribution does not create a net flow of the liquid. The precise form of the kernel is not available. We used the following phenomenological kernel expressed by its Fourier transform:

$$\hat{K}(k) = \int \exp[i\mathbf{k}\mathbf{r}]K(r)d\mathbf{r} = \exp[-\kappa(E)k^2 - k^4 d_0^4]. \qquad (9)$$

This form is justified by the spatial homogeneity (dependence of k^2 only), normalization $[\hat{K}(0) = \int K(r')d\mathbf{r}' = 1]$, and the locality conditions (rapid decays for $k > 1/d_0$, where d_0 is the characteristic length of the order of the electrodes separation). The field dependent factor $\kappa(E)$ describes the experimentally observed transition from the short-wave instability at small fields (honeycombs for $\kappa < 0$) to long-wave instability at larger fields (coarsening, coalescence, and attraction of toroidal vortices for $\kappa > 0$). After combining Eqs. (6), (8), and (9) one obtains

$$\partial_t V = \nu\nabla^2 V - \zeta V - cE\int K_1(|\mathbf{r} - \mathbf{r}'|)(\rho_p + \rho_g)d\mathbf{r}', \qquad (10)$$

where the Fourier transform $\hat{K}_1 = 1 - \exp[-\kappa(E)k^2 - k^4 d_0^4]$. We also scaled away s.

The function f has a different structure for low concentrations ($c \ll 1$) and high concentrations. For $c \rightarrow 0$ this function must coincide with that derived in Ref. [4]:

$$f_1 = (\rho_p - \rho_*) \times \begin{cases} \rho_p, & \text{if } 0 \leq \rho_p \leq \rho_*, \\ C_*\rho_g(1 - \rho_p), & \text{if } \rho_* \leq \rho_p \leq 1, \end{cases} \qquad (11)$$

where the constants $C_* \sim O(1)$ and $\rho_*(E)$ are discussed in Ref. [4]. Experiments for higher values of c suggest that both ρ_g and ρ_p tend to some equilibrium value determined by the electric field E. To confirm this statement we carried out a special experiment in a relatively small cell (high $d = 3$ mm, length 5 mm, and spacing between transparent side walls 1 mm). In this cell observations

were performed from the side, providing the possibility to count "gas" N_g and "precipitate" N_p particles. Moreover, due to the reduced cell size the large-scale hydrodynamics flows are suppressed. The results of the experiments are shown in the Fig. 1 inset. As one sees that the number of gas particles N_g near the critical field E_0 behaves as $N_g \sim E - E_0$ independently on the total number of particles in the cell $N = N_g + N_p$. For larger fields $N_g \to N$. It implies the following relation $N_g = \mu(E)N_p/N$, $\mu(E) \sim E - E_0$, or $N_g = \mu(E)/[1 + \mu(E)/N]$. This dependence appears to be in excellent agreement with the experimental data; see Fig. 1, inset. Thus, in accord with the experimental data, f can be written as

$$f_2 = cC_2[\rho_g - \mu(E, q)\rho_p/\bar{\rho}]. \tag{12}$$

Here C_2 characterizes the relaxation towards the equilibrium and $\bar{\rho} = \langle \rho_g + \rho_p \rangle = \mathrm{const}$ is the mean density. In steady state f_2 enforces the relation between the densities $\rho_g/\rho_p \to \mu/\bar{\rho}$. Here we also included in μ the dependence on local charge distribution q. We set for the simplicity $q = \mathrm{const}$. However, the convective flows will affect the ions density, which will shift the gas/precipitate equilibrium, see [5]. This effect can be modelled by including the dependence of μ on V. We used the following expression $\mu = \mu_0(E)[\tanh(\mu_1 \mathrm{sgn}(E)V) + 1]$. It incorporates the observation that gas concentration is suppressed by rising flows for $E < 0$. We applied a hybrid form for f valid for arbitrary c:

$$f = f_2 + \exp[-c/c_0]f_1, \tag{13}$$

where c_0 is some "crossover" concentration.

Stability of homogeneous precipitate.—For $E \to E_0$ we can set $\mu \to 0$, i.e., equilibrium gas density $\rho_g \to 0$. Then the stability of the precipitate (i.e., homogeneous "Wigner" crystal state in experiment) $\rho_p = \bar{\rho}$ can be readily performed because the equation for ρ_g splits off and the analysis is reduced to Eqs. (1) and (10) for ρ_p. We will focus on the case of high concentration $c \gg c_0$ and neglect the last term in Eq. (13) (the case of $c = 0$ was considered in Ref. [4]). In the linear order for periodic perturbations V, $\rho_p \sim \exp[\lambda t + ikx]$, Eqs. (1) and (10) yield

$$\lambda V = -(\nu k^2 + \zeta)V + E(1 - \exp[-\kappa(E)k^2 - k^4 d_0^4])\rho_p,$$
$$\lambda \rho_p = -D_p k^2 \rho_p - \alpha_p \beta \bar{\rho}(1 - \beta\bar{\rho})V. \tag{14}$$

The growth rate $\lambda(k)$ depends on the sign of the field E; see Fig. 1. For negative E and $\kappa < 0$ in a certain parameter range λ is positive in a narrow band near the optimal wave number k_0, which is the hallmark of short-wave instability. In this regime our solution indicates the formation of stable honeycomb lattice with the scale determined by k_0. For the same parameters, but for $E > 0$ the homogeneous state $\rho_p = \bar{\rho}$ is stable (dashed line in Fig. 1). This observation is consistent with the experimental fact that field reversal transforms the honeycomb to the ho-

mogeneous precipitate and vice versa. With the increase of E and κ the left edge of the unstable band of $\lambda(k)$ crosses zero and long-wave instability ensues. This regime corresponds to the coalescence of clusters.

A qualitative phase diagram is shown in Fig. 2. The positions of transition lines are approximate because the field dependence of κ, μ_0, and β is not available at the moment. To describe the observed phenomenology, we only assumed that κ, μ_0, and ρ_* monotonically increase with the increase of E, and the functions $\alpha_{g,p}$, β decrease ($1/\beta$ is the limiting density of the t vortex which increases with the increase of E). The line $\lambda = 0$ for short-wavelength instability for $E < 0$ depicts the transition to honeycombs. The transition from honeycombs to pulsating rings is identified as a transition from short-wave to long-wave instability, which roughly coincides with $\kappa(E) = 0$. This transition is associated with an overall increase of gas concentration [increase of $\mu(E)$] and a decrease of β (increase of maximum density of ρ_p). The transition from static clusters to dynamic structures and honeycombs occurs approximately with the increase of concentration c at $c = c_0$. For $E > 0$ the transition from stable precipitate to "down t vortices" is approximately given by $\kappa(E) = 0$. In this case there is no distinction between the "immobile" and the "Wigner crystal" because our model does not take into account the friction and adhesion.

The numerical solution of Eqs. (1) and (10) was performed by the quasispectral method based on fast Fourier transformation (FFT). Typically 256×256 FFT harmonics in periodic boundary conditions were used. For $c > c_0$, $E < 0$, and $\kappa < 0$, corresponding to the case of the short-wavelength instability, we observed the spontaneous formation of honeycomb lattice from random initial conditions; see Fig. 3. For the same parameters but $E > 0$ the homogeneous state $\rho_p = \mathrm{const}$ (Wigner crystal) was stable. With the increase of E and for $\kappa > 0$ (i.e., in the case of long-wavelength instability) we observed the
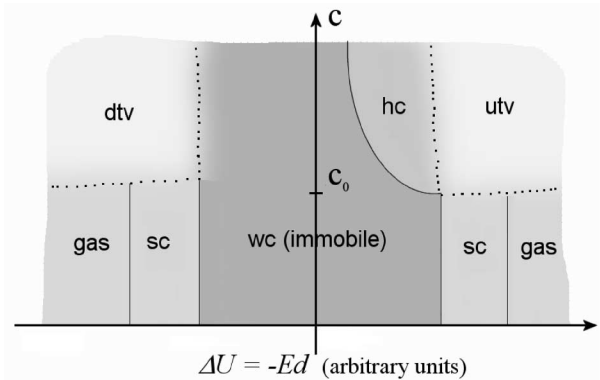

FIG. 2. Qualitative phase diagram, $\Delta U = -Ed$ is applied voltage (plus on top plate), c is the concentration of the additive. Domain sc: static clusters; wc: stable homogeneous precipitate (Wigner crystals); hc: honeycombs; utv and dtv: up/down toroidal vortices.
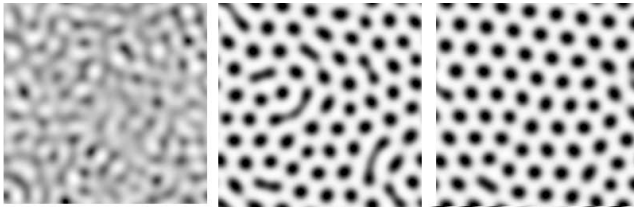
FIG. 3.   Formation of honeycomb, shown snapshots of ρ_p for $\bar{\rho} = 0.3$, $\nu = 2$, $E = -50$, $\alpha = 0.02$, $\mu_0 = 0$, $C_1 = 5$, $c = 1$, $c_0 = 0.1$, $C_* = 10$, $D_p = 1$, $d_0 = 1$, $\alpha_p = -\alpha_g = -0.6$, $\kappa = -0.1$, and $\beta = 2$, domain of integration 80×80 dimensionless units. Images from left to right: $t = 10$, 400, and 2000. Black corresponds to $\rho_p = 0$, white to $\max(\rho_p)$. See also movie 1 in [8].

transition from honeycombs/Wigner crystals to the regime of cluster attraction and coalescence. In this case the EHD flows accelerate the coarsening process of the t vortices.

In the course of coalescence the vortices grow and become unstable, producing pulsating rings for $E < 0$ and rotating objects for $E > 0$, Figs. 4 and 5. The instability in both cases is caused by the dynamic coupling between the particles density and vertical flows described by the function f. For $E < 0$, i.e., for the up toroidal vortices, the vortices are primarily built of a low-mobile precipitate phase with a small amount of gas above them. The instability occurs in the bulk of the vortex, resulting in the formation and breaking up of "gas bubbles" inside the precipitate. For $E > 0$ the vortices are formed by a mobile gas phase with a small content of precipitate. The instability occurs at the vortex edge yielding counter-propagating clock/anticlock waves of shape deformation. Eventually one wave survives, creating the effect of rotation.

In our experiments we observed also the multipetal vortices exhibiting almost a solid-state rotation. These multipetal vortices generate horizontal flow of the liquid which is neglected in our theory. We believe that the vertical vorticity is in fact the consequence rather than the reason of rotation. It is likely that the vortex shape instability present in our model eventually triggers the rotation of surrounding fluid and generates vertical vor-
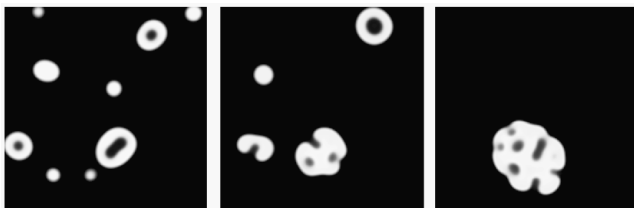

FIG. 4.   Evolution of pulsating rings, shown snapshots of ρ_p for $\bar{\rho} = 0.18$, $\nu = 2$, $E = -70$, $\alpha = 0.02$, $\mu_0/\bar{\rho} = 0.25$, $\mu_1 = 0.5$, $C_1 = 5$, $c = 1$, $c_0 = 0.1$, $C_* = 10$, $D_p = 1$, $D_g = 5$, $d_0 = 1$, $\alpha_p = -\alpha_g = -0.15$, $\kappa = 0.1$, and $\beta = 0.5$, domain of integration 80×80 units. Images from left to right: $t = 450$, 1120, and 3000. See also movies 2 and 6 in [8].
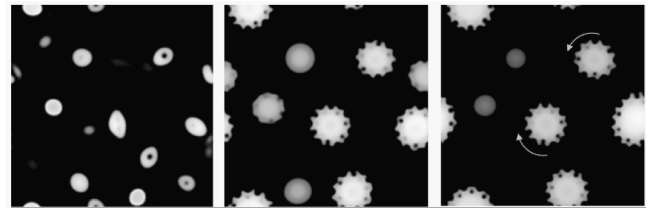
FIG. 5.   Rotating down t vortices, shown snapshots of ρ_p for $\bar{\rho} = 0.18$, $\nu = 2$, $E = 160$, $\alpha = 0.02$, $\mu_0/\bar{\rho} = 19.5$, $\mu_1 = 0.5$, $C_1 = 0.45$, $c = 1$, $c_0 = 0.1$, $C_* = 10$, $D_p = 1$, $D_g = 5$, $d_0 = 1$, $\alpha_p = -\alpha_g = -0.15$, $\kappa = 0.1$, and $\beta = 0.5$, domain of integration 150×150 units. Images from left to right: $t = 16$, 320, and 540. See also movies 3 and 7 in [8].

ticity. Explicit incorporation of the vertical vorticity likely will not change the qualitative features.

We develop the phenomenological continuum theory of pattern formation and self-assembly of metallic microparticles immersed in a poorly conducting liquid. This theory reproduces primary patterns observed in the experiment and leads to an interesting prediction of the relation of rotation with the vortex edge instability. The parameters of the model can be extracted from the molecular dynamics simulations and the generalization of the "leaky dielectric model" [9] and validated by the experiments.

[1] R. C. Hayward, D. A. Saville, and I. A. Aksay, Nature (London) **404**, 56 (2000); M. Trau *et al.*, Nature (London) **374**, 437 (1995); S.-R. Yeh, M. Seul, and B. I. Shraiman, Nature (London) **386**, 57 (1997).

[2] R. B. M. Schasfoort *et al.*, Science **286**, 942 (1999); A. R. Minerick, A. E. Ostafin, and H.-C. Chang, Electrophoresis **23**, 2165 (2002).

[3] I. S. Aranson *et al.*, Phys. Rev. Lett. **84**, 3306 (2000).

[4] I. S. Aranson, B. Meerson, P. V. Sasorov, and V. M. Vinokur, Phys. Rev. Lett. **88**, 204301 (2002).

[5] M. V. Sapozhnikov, Y. V. Tolmachev, I. S. Aranson, and W.-K. Kwok, Phys. Rev. Lett. **90**, 114301 (2003).

[6] J. F. Richardson and W. N. Zaki, Trans. Inst. Chem. Eng. **32**, 35 (1954); C. Y. Wen and Y. H. Yu, Chem. Eng. Prog., Symp. Ser. **62**, 100 (1966).

[7] L. D. Landau and E. M. Lifshits, *Fluid Mechanics* (Pergamon Press, New York, 1987).

[8] See EPAPS Document No. E-PRLTAO-92-032422 for movies which illustrate the formation and dynamics of various states in electrostatically driven granular media. A direct link to this document may be found in the online article's HTML reference section. The document may also be reached via the EPAPS homepage (http://www.aip.org/pubservs/epaps.html) or from ftp.aip.org in the directory /epaps/. See the EPAPS homepage for more information.

[9] D. A. Saville, Annu. Rev. Fluid Mech. **29**, 27 (1997).